Integrated genomic and epigenomic analyses pinpoint biallelic gene inactivation in tumors

Giuseppe Zardo[1,2*], Maarit I. Tiirikainen[1,2*], Chibo Hong[1,2], Anjan Misra[1–3], Burt G. Feuerstein[1–3], Stanislav Volik[1,4], Colin C. Collins[1,4], Kathleen R. Lamborn[1,2], Andrew Bollen[1,5], Daniel Pinkel[1,3], Donna G. Albertson[1,4] & Joseph F. Costello[1,2]

*These authors contributed equally to this work.

Published online 30 September 2002; doi:10.1038/ng1007

Aberrant methylation of CpG islands and genomic deletion are two predominant mechanisms of gene inactivation in tumorigenesis, but the extent to which they interact is largely unknown. The lack of an integrated approach to study these mechanisms has limited the understanding of tumor genomes and cancer genes. Restriction landmark genomic scanning (RLGS; ref. 1) is useful for global analysis of aberrant methylation of CpG islands, but has not been amenable to alignment with deletion maps because the identity of most RLGS fragments is unknown. Here, we determined the nucleotide sequence and exact chromosomal position of RLGS fragments throughout the genome using the whole chromosome of origin of the fragments[2] and *in silico* restriction digestion of the human genome sequence. To study the interaction of these gene-inactivation mechanisms in primary brain tumors, we integrated RLGS-based methylation analysis with high-resolution deletion maps from microarray-based comparative genomic hybridization (array CGH; ref. 3). Certain subsets of gene-associated CpG islands were preferentially affected by convergent methylation and deletion, including genes that exhibit tumor-suppressor activity, such as *CISH1* (encoding *SOCS1*; ref. 4), as well as genes such as *COE3* that have been missed by traditional non-integrated approaches. Our results show that most aberrant methylation events are focal and independent of deletions, and the rare convergence of these mechanisms can pinpoint biallelic gene inactivation without the use of positional cloning.

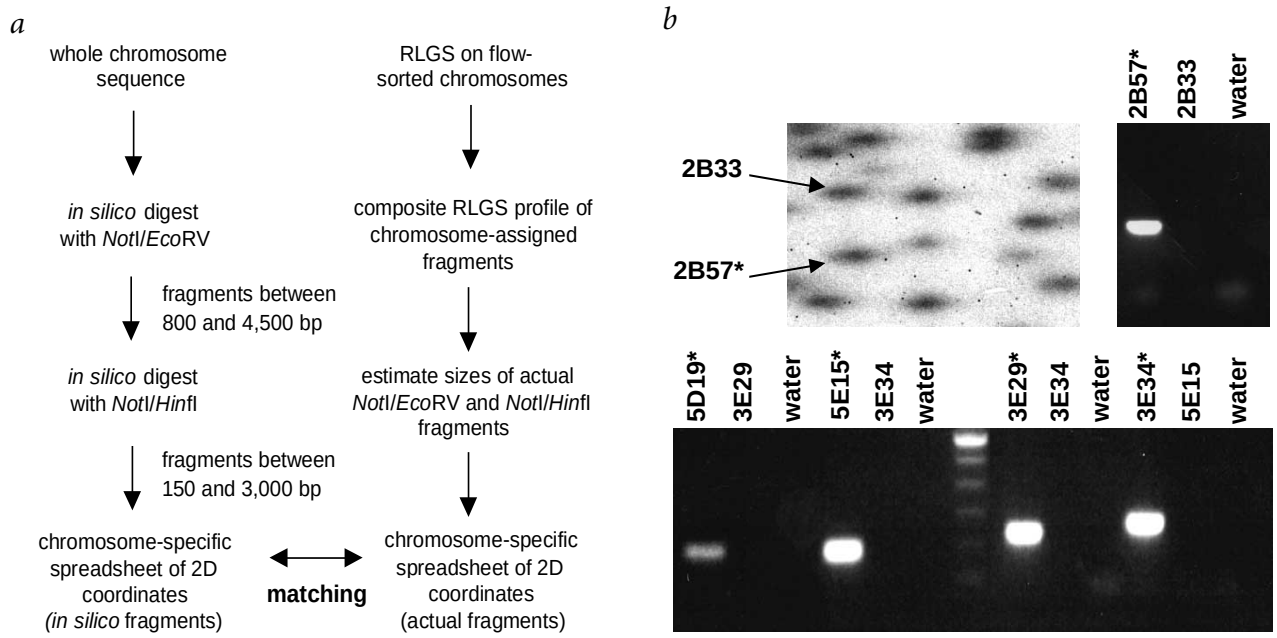

Fig. 1 Identification of the sequences and precise chromosomal localizations of RLGS fragments. ***a***, Strategy for matching *in silico* *Not*I fragments generated from the human genome sequence (left side) to actual RLGS fragments (right side) on the basis of chromosome of origin and estimated two-dimensional size of each fragment. ***b***, PCR confirmation of matches, using primers designed from the sequence of the predicted matched fragment. DNA templates for PCR were individual fragments excised from the RLGS gel (top, left) and included the putative matched fragment (marked with an asterisk) and unrelated negative control fragments or water only (top, right). Lower panel, PCR products confirming four additional predicted matched fragments.

[1]*Comprehensive Cancer Center,* [2]*The Brain Tumor Research Center and Department of Neurological Surgery,* [3]*Department of Laboratory Medicine,* [4]*Cancer Research Institute and* [5]*Department of Pathology, University of California, San Francisco, San Francisco, California 94115, USA. Correspondence should be addressed to J.C. (e-mail: jcostello@cc.ucsf.edu).*

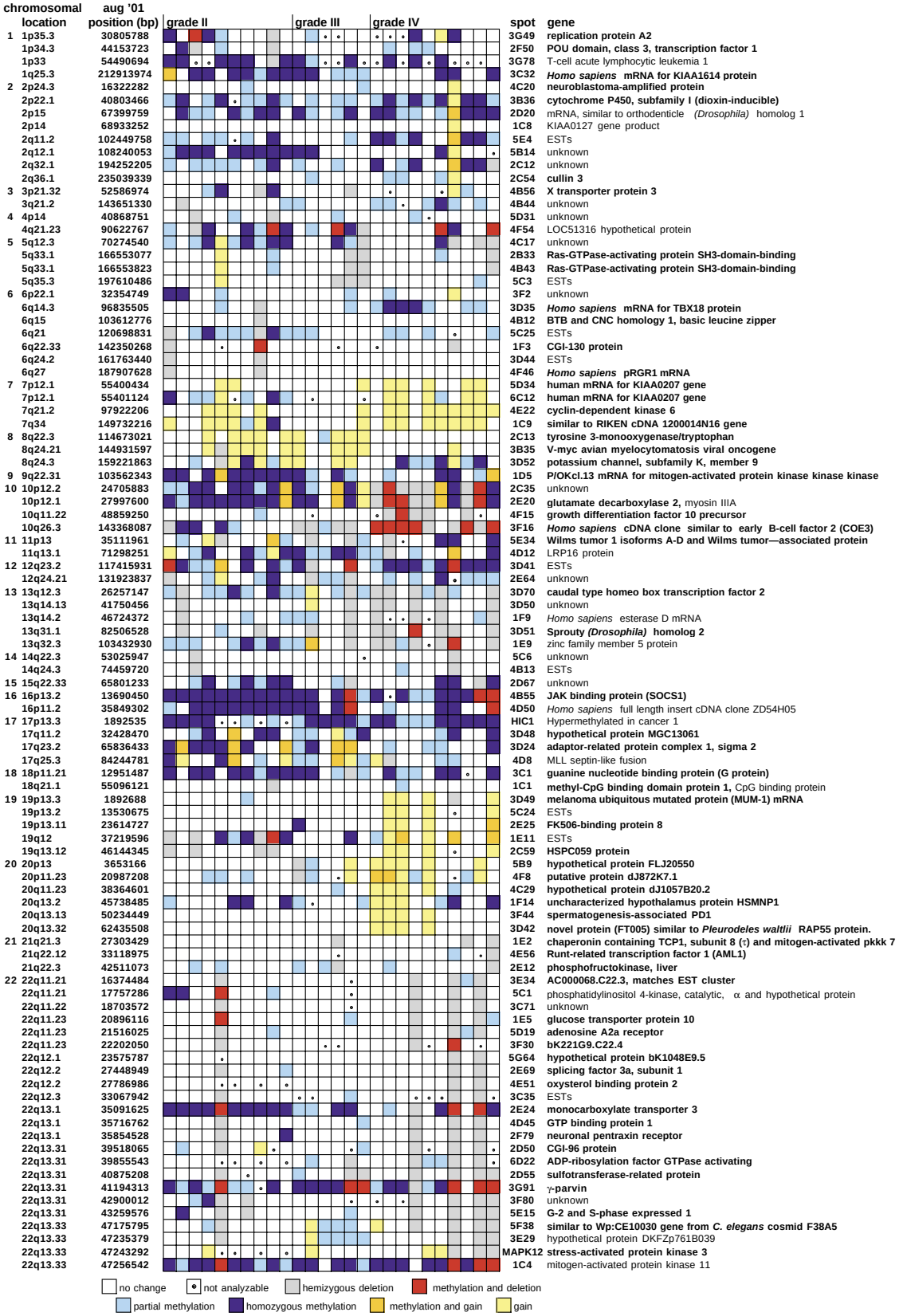

Fig. 2 Aberrant methylation and gain or loss of copy number in 26 human gliomas. Gene names in bold indicate that the *Not*I fragment (spot) is in the 5′ region. The two genes with the highest incidence of convergent methylation and deletion were 5′ CpG islands 3G91 and 3F16. The total number of methylation-and-deletion (MD) events was similar between putative 5′ and non-5′ sites, with 60% (27 of 45) of MD events in 5′ CpG islands and 40% (18 of 45 events) in non-5′ CpG islands. RLGS spots were given three-variable coordinates for identification purposes (see Web Fig. A online). Fragments that were potentially imprinted or commonly polymorphic at the restriction sites (fragments that vary between 'diploid intensity', 50% reduction and complete absence of a spot) in normal tissue were excluded from the analysis. The samples, from left to right, were: grade II; 1A, 2A, #6, #7, #8, #20, #22, #23, #24, #25, grade III: #1, #2, #4, #7, #8, #10, grade IV; #1–9, #15.

An integrated approach for mapping genomic and epigenomic alterations across tumor genomes is crucial for identifying candidate tumor-suppressor genes. Identifying such genes by either deletion mapping or methylation analysis alone has been problematic, and most work has focused on single regions identified by positional cloning and evaluation of candidate genes. These studies have established that methylation and deletion do converge on individual tumor-suppressor genes[5,6]. To develop a genome-wide approach for mapping genomic and epigenomic alterations, we combined RLGS, a two-dimensional gel-based method of analyzing the methylation status of thousands of genes containing CpG islands[1], with high-resolution analysis of DNA copy number, array CGH (refs 3,7) and quantitative microsatellite analysis (QuMA; ref. 8). In RLGS, DNA is cleaved with the methylation-sensitive enzyme *Not*I and with *Eco*RV and radioactively labeled at the cleaved *Not*I sites. After size separation in the first dimension, DNA is further digested with *Hin*fI and separated by electrophoresis in a second dimension to generate a reproducible profile of more than 1,000 spots (see Web Fig. A online). The intensity of each spot reflects the methylation status and copy number of the fragment[9–13]. Because the identities of most of the RLGS loci are unknown, precluding their alignment with copy-number maps of chromosomes, we developed a custom PERL program to generate RLGS digestion fragments from the human genome sequence, similar to an informatics tool termed Virtual Genome Scan[14]. We matched *in silico* restriction fragments with actual RLGS fragments on the basis of their two-dimensional fragment size and chromosome of origin[2] and confirmed each match by PCR (Fig. 1). Here, we applied this RLGS map, comprised of all RLGS fragments from chromosome 22 and 2–8 RLGS loci from all other somatic chromosomes, to the analysis of brain tumors (Fig. 2).

To measure the interaction of methylation and deletion at the 96 loci, we analyzed DNA from 26 human brain tumors by RLGS, array CGH and QuMA (see Web Table A online for QuMA results). We attributed RLGS fragment loss (decreased intensity) to (i) partial methylation, if the decrease in *Not*I fragment intensity was at least 30% but less than 70%, relative to normal brain, and deletions were not observed; (ii) homozygous methylation, if the decrease in *Not*I intensity exceeded 70% and no deletions were observed; (iii) deletion, if the *Not*I fragment intensity was decreased by approximately 50%, and deletion was observed; or (iv) methylation and deletion, if the decrease in *Not*I fragment intensity was more than 70%, and hemizygous deletion was indicated. Using these criteria, we found that aberrant CpG island methylation rarely occurred together with deletion (45 events in 2,406 sites, 1.8%, or, excluding sites with no alteration, 45 events in 989 sites, 4.6%; Fig. 2). For ten loci, however, we detected recurrent convergence of deletion and methylation. If these patterns of biallelic alteration were random, it is unlikely that the events would have a functional impact on tumorigenesis. But the pattern of convergence is non-random ($P < 0.001$; Fig. 3*a*), suggesting that some of these events arise through growth selection, increased locus-specific susceptibility to deletion and methylation, or both.

We also examined the pattern of gain-and-methylation events in these tumors (Fig. 3*b*). The analysis indicated that a subset of CpG islands were preferentially altered by such events ($P < 0.001$). The data suggest that some aberrant CpG island methylation may mitigate the effect of copy-number gain in tumors, although this remains to be tested.

We found that the RLGS fragment 4B55, corresponding to *CISH1* (also known as *SOCS1*) at 16p13.2 (refs 15,16), was aberrantly methylated on both alleles in 18 of 26 tumors (Fig. 2). In a further three tumors, including one grade IV tumor with a relatively small deletion (approximately 3.16 Mb), the locus was both methylated and deleted. Our genomic and epigenomic analyses indicating that the locus is affected in almost all brain tumors in this small set of samples, together with other observations identifying methylation of *CISH1* in hepatocellular carcinoma and functional assays implicating CISH1 in growth control[4], implicates *CISH1* as a candidate tumor-suppressor gene.

We found a second locus, 3F16 at 10q26.3 (a region frequently deleted in grade IV tumors[17–20]), to be aberrantly methylated and deleted in our grade IV tumors and homozygously methylated in grade II tumors (Fig. 4*a*). This fragment maps to the 5′ end of the putative *COE3*, a member of the COE family of transcription factors that regulate neurogenesis and differentiation[21]. *COE3* is expressed in normal adult brain but repressed in four glioma cell lines (Fig. 4*b*). We were able to reactivate *COE3* expression by treating cells with the demethylating agent 5-aza-2-deoxycytidine, suggesting that aberrant methylation caused silencing of *COE3*. Consistent with this, a more in-depth bisulfite-sequencing analysis showed that *COE3* was extensively methylated in cells with little or no *COE3* expression and was unmethylated in normal brain (Fig. 4*c*).

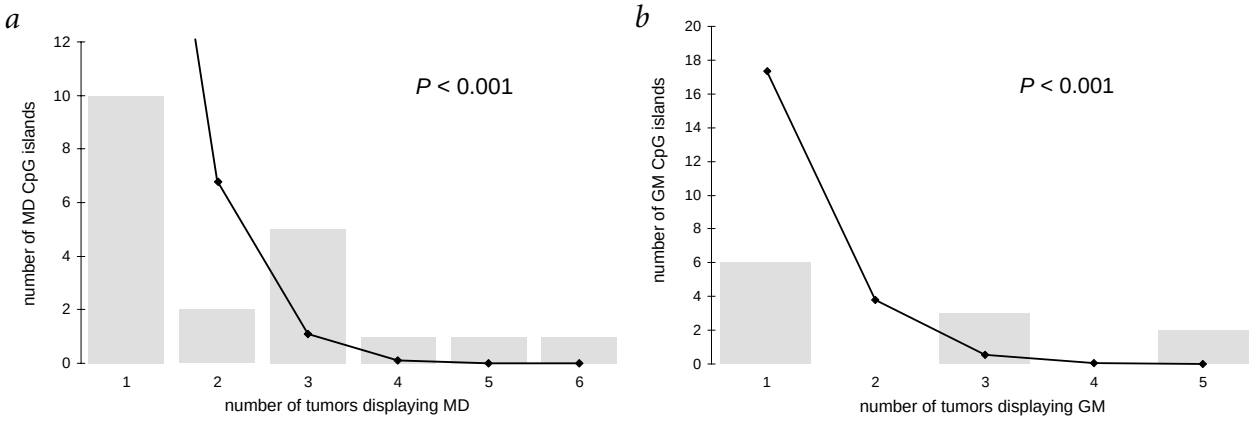

Fig. 3 Subsets of CpG islands were preferentially altered by converging genomic and epigenomic mechanisms. The histograms display the number of tumors (of 26 total) in which the particular CpG islands were either (***a***) methylated and deleted (MD events) or (***b***) gained and methylated (GM events). The line plot in each panel represents the expected distribution assuming that all CpG islands have an equal frequency of alteration. For example, there are five CpG islands that exhibit MD in three of the tumors, whereas from a random pattern only one such CpG island would be expected. *P* values indicate that the observed and expected frequencies of alteration were significantly different from one another.

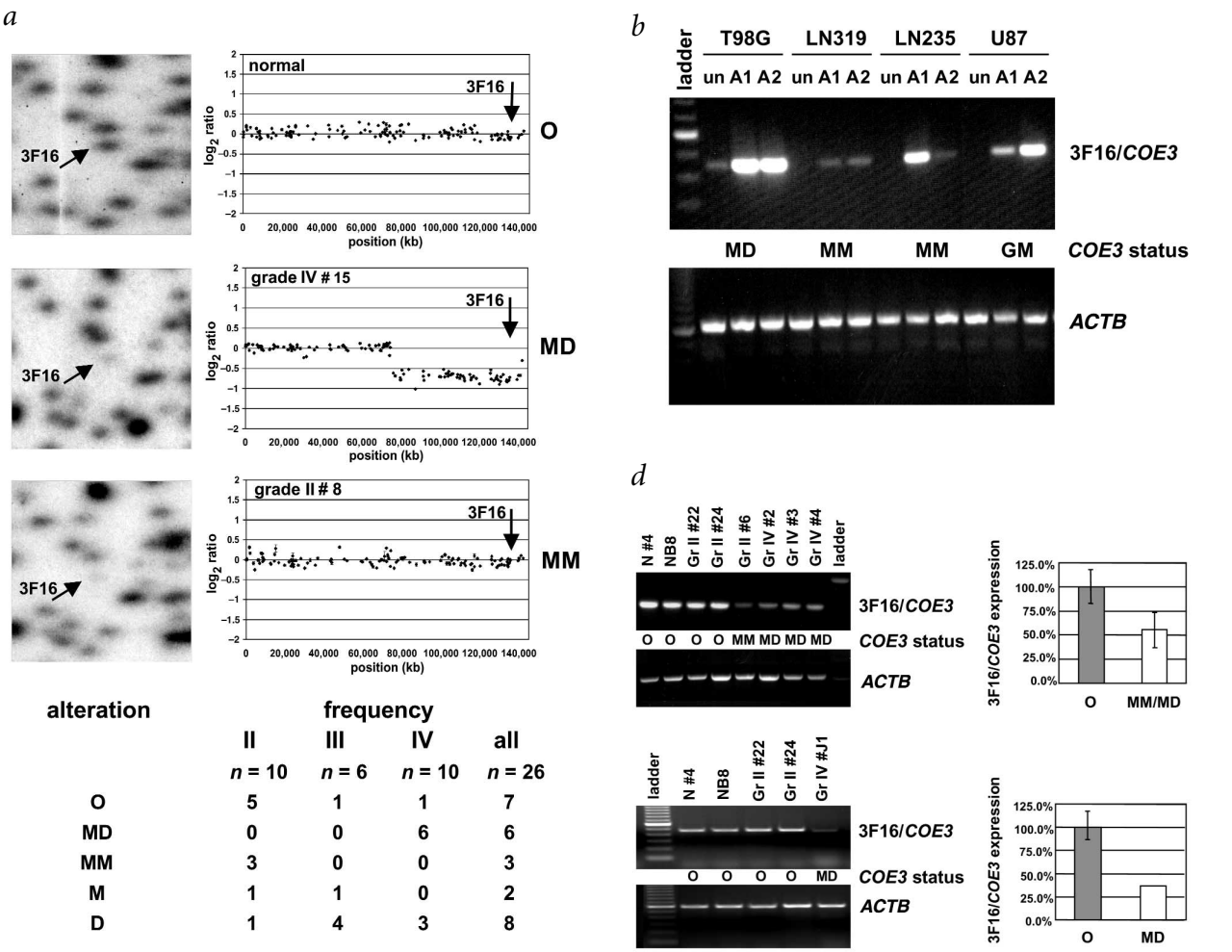

alteration	frequency			
	II	III	IV	all
	n = 10	*n* = 6	*n* = 10	*n* = 26
O	5	1	1	7
MD	0	0	6	6
MM	3	0	0	3
M	1	1	0	2
D	1	4	3	8

Fig. 4 Aberrant methylation and deletion at putative *COE3* (fragment 3F16). ***a***, RLGS profiles highlighting the *COE3* *Not*I fragment (→) along with the *COE3* locus (↓) on the copy-number plot from the same tumor. Lower panel, summary of *COE3* alterations, grades II–IV. O, no alteration; M, partial methylation; MM, homozygous methylation; D, hemizygous deletion; MD, methylation and deletion. ***b***, RT–PCR analysis of *COE3* and *ACTB* expression in four human glioma cell lines. un, untreated cells; A1, A2, independent treatments of cells with 1 μM 5-aza-2-deoxycytidine for 3 d. The *COE3* status prior to demethylation treatment is listed. ***c***, Analysis of the methylation status of *COE3* in normal brain (NB3, NB7, NB8) and brain tumor cell lines determined by the bisulfite-sequencing method. Each row of circles represents sequence analysis of an individual clone from the PCR product (open circle, unmethylated CpG; filled circle, methylated CpG). CpG 41 and 42 are within the original *Not*I site. ***d***, RT–PCR analysis of *COE3* and *ACTB* expression in normal brain from two different individuals (N#4, NB8) and in primary brain tumors with and without *COE3* alteration. The graphs display the statistically significant difference ($P = 0.013$) in average and standard deviation of the amount of RT–PCR product (ratio of *COE3* to *ACTB*) in tumors with alteration (MM/MD) relative to that in normal brain and tumors without alteration (O). The lower panel shows an independent analysis of the samples without *COE3* alteration along with an additional grade IV brain tumor (J1) exhibiting methylation and deletion of *COE3*. We expected that all samples would exhibit some *COE3* expression, as each contains a fraction of non-tumor cells, particularly blood cells that express *COE3* at a significant level (see Web Fig. C online).

COE3 expression was also significantly lower ($P = 0.013$) in primary brain tumors with biallelic alteration (Fig. 4*d*). Thus, *COE3* is a novel target of biallelic inactivation in brain tumors and has been missed by traditional approaches. This raises the possibility that there may be additional undetected genes with a similar pattern of biallelic inactivation in tumors.

In summary, our integrated approach addresses a large gap in the understanding of tumor genomes. Mapping RLGS fragments *in silico* is widely applicable to all chromosomes and enzyme combinations. These maps will facilitate a more comprehensive assessment of DNA copy number and methylation and provide a new capability for genome-wide analyses of methylation and gene expression. In contrast with candidate-gene studies, our global approach suggests that aberrant methylation and deletion primarily affect separate sets of genes in brain tumors.

Methods

Tumor samples. We obtained 26 glioma samples and 11 non-tumor brain samples from the Neurosurgery Tumor Bank at the University of California, San Francisco. The samples included ten grade II gliomas (as graded by the World Health Organization (WHO)), six grade III anaplastic astrocytomas and ten grade IV glioblastomas (eight primary and two recurrent; Fig. 2). We obtained 11 non-tumor brain samples from different individuals, including two samples of brain adjacent to tumor (BAT4, BAT6), one autopsy sample (N#4) and eight surgical samples from individuals with epilepsy (NB1–8). Samples were obtained with informed consent and their use was approved by the Committee on Human Research at University of California, San Francisco.

RLGS. We did RLGS according to published protocols[1]. Briefly, non-specific sheared ends of 1–3 μg of genomic DNA were blocked in a 10-μl reaction by the addition of nucleotide analogs (αS-dGTP, αS-dCTP, ddATP, ddTTP) with 2 U DNA polymerase I (37 °C, 20 min) followed by enzyme inactivation (65 °C, 30 min). We adjusted the buffer and digested DNA (37 °C, 2 h) with 20 U *Not*I (Promega), which is sensitive to methylation. We then used Sequenase (version 2.O, U.S.B.) to fill in the *Not*I ends with [α-^{32}P]dGTP and [α-^{32}P]dCTP (Amersham) for 30 min at 37 °C. We digested the labeled DNA (37 °C, 1 h) with 20 U *Eco*RV (Promega) and separated a portion by electrophoresis through a 60-cm long, 0.8% agarose tube gel (first-dimension separation). The agarose gel was next equilibrated in *Hin*fI digestion buffer, and the DNA was digested in the gel with 700 U *Hin*fI (Promega) at 37 °C for 2 h. We then placed the agarose gel horizontally (rotated 90° relative to the first direction of electrophoresis) across the top of a non-denaturing 5% polyacrylamide gel, connected the two gels with molten agarose and separated the DNA by electrophoresis in the second dimension. We dried the gels and exposed them to X-ray film in the presence of intensifying screens (Quanta III, DuPont) for 2–10 d. We carried out RLGS at least twice for each tumor, except for three of the grade III samples.

RLGS coordinate system. Each radioactively labeled *Not*I fragment displayed on the typical *Not*I/*Eco*RV (first-dimension) and *Not*I/*Hin*fI (second-dimension) profile was assigned a three-variable designation consisting of its *y* coordinate, *x* coordinate and fragment number. For example, 3C21 represents *y* coordinate 3, *x* coordinate C and fragment number 21 (see Web Fig. A online).

RLGS profile analysis. We compared profiles of tumor and normal brain DNA (from three unrelated individuals, BAT4, BAT6, N#4) by visual inspection of overlaid autoradiographs and corroborated them using a two-dimensional gel analysis program (Non-linear Dynamics). To diminish the contribution of common restriction-site polymorphism to apparent spot loss, we selected only those spots that were consistently present in profiles from normal brain (three individuals), peripheral blood lymphocyte DNA (three individuals) and normal muscle (four individuals). This technique also distinguished methylation due to normal imprinting from abnormal methylation in the tumors. Our two-dimensional gel analysis program automatically detected, matched and quantified spots, and used 'mode of non-spot' for background correction. To normalize differences in DNA loading and autoradiography times, the program calculated the ratio of the volume of each spot to the sum of the volumes of at least 900 single-copy spots in the normal and tumor profiles, and then calculated the ratio of these ratios. The program output graphically the results of the quantification (see Web Fig. B online). We used these software-derived values and visual inspection to determine the alteration status for each data point (as described earlier), with visual inspection overriding the software in numerous cases. The actual average spot intensity for the categories of alteration in the tumors were as follows: relative to normal brain (100%), the intensity for partial methylation was 50.7%, for methylation and deletion, 10.8%, for homozygous methylation, 16.7% and for hemizygous deletion, 65%. The high average for deletion events is a result of the conservative criteria required for an event to be considered methylation and deletion. Although some alterations were near the threshold values, and thus could be considered either deletion or methylation and deletion, the average values and distribution of intensities indicate that the vast majority were clearly classified as one type or the other. Criteria for the category of methylation and deletion were particularly stringent, requiring evidence of deletion by both array CGH and RLGS and also that approximately 40% of the remaining allele (20% of remaining 50%, or 70% spot loss in total) be methylated. For approximately 20% of spots, there was disagreement between spot intensity assessed visually and quantified with the software. This reflects the limitation of the software in accurately quantifying spots that are very close to other spots, diffuse spots or spots with a high local background. Visual assessment was more reliable in these cases. In no case was the software quantification used without visual assessment.

***In silico* digests.** We used the August 2001 freeze of the University of California, Santa Cruz version of the draft assembly of human genome for the *in silico* restriction analysis. Briefly, we downloaded the whole-chromosome assemblies and analyzed them using a custom PERL program on a Sun Ultra 80 workstation. The program accepted as arguments the name of a FASTA sequence file to be analyzed and the names and recognition sites of the restriction endonucleases that were used for generation of experimental RLGS profiles. The results were output to a FASTA file with predicted fragment sequences, the two-dimensional size for each fragment and the nucleotide position along the chromosome. This tab-delimited file could be directly imported into commercial spreadsheet analysis programs such as Microsoft Excel. The program can be adjusted for any restriction enzyme combination, and can process the human genome in less than one hour, facilitating consecutive analysis of each version of the genome assembly as it becomes available. We generated similar spreadsheets of actual fragments by determining the whole chromosome of origin of each fragment from RLGS analysis of flow-sorted human chromosomes[2] and estimating the two-dimensional size of each fragment based on the exact known sizes of previously cloned fragments. We then matched the *in silico* fragments with the actual fragments based on two-dimensional size and chromosome of origin.

PCR confirmation of sequence assignments. We excised individual *Not*I fragments from an RLGS gel containing human genomic DNA. DNA was eluted in 0.5 M ammonium acetate, pH 8, 1 mM EDTA (150 μl) at 37 °C overnight and precipitated with 2.5 volumes of cold ethanol at –70 °C overnight using 1 μg glycogen as carrier. We resuspended DNA in 10 μl of 10 mM Tris–HCl, pH 8.0, 1 mM EDTA buffer. We amplified 1 μl of each sample by PCR (35 cycles) using primers derived from the sequences predicted for each *Not*I/*Hin*fI fragment. We tested the specificity of the PCR reaction using water and unrelated spot DNA.

Array CGH. To determine the copy number across all chromosomes, we did comparative genomic hybridizations on whole-genome arrays of approximately 2,400 chromosomally mapped BAC clones (HumArray1.14) following previously described methods (ref. 3; see Web Table A online). Briefly, we hybridized arrays simultaneously with 600 ng each of tumor DNA labeled with Cy3–dCTP by random priming and Cy5–labeled reference DNA from normal brain tissue. We counterstained the spotted BAC DNA with 4′,6′-diamidino-2-phenylindole hydrochloride (DAPI) and collected and processed the images of the three fluorochromes using custom software[7] that calculates the raw ratios and mean $\log_2$ ratios of triplicates of tumor to reference DNA hybridization. After normalization, we plotted mean $\log_2$ ratios and analyzed the resultant graphs for deletions and gains along each chromosome.

QuMA. To corroborate the array CGH results, we also assessed copy number with 17 microsatellite markers from chromosome 22 using a previous-

ly described real-time PCR-based method[8]. Briefly, we amplified triplicates of each DNA sample (5 ng) simultaneously with primers specific for each microsatellite marker and with pooled reference primers in separate wells. We measured the accumulation of PCR product using a dual-labeled fluorogenic oligonucleotide TaqMan probe, 5′-(FAM)-TGTGTGTGTGTGTG TGTGTGT-(TAMRA)-3′, which detects the CA repeats in the PCR products. The reporter (FAM) fluorescence is liberated from the quencher (TAMRA) as a PCR product is generated, and serves as a direct measure of the amount of PCR product. To measure the relative copy number of the tumor sample compared with normal DNA, we did control reactions on normal brain tissue from nine different individuals.

The names and positions of the markers (based on the August 2001 freeze of the draft human genome from University of California Santa Cruz) are shown in Web Table A online. The genomic positions of three microsatellite markers (*D22S539*, *D22S1150*, *D22S426*) overlapped exactly with three array CGH BAC clones (at 18,956 kb, 26,197 kb and 33,638 kb). We selected seven additional markers used in a reference PCR pool from genomic positions that are typically unaffected in gliomas (*D8S1715* at 8p21.3, *D2S391* at 2p21, *D1S210* at 1q23-24, *D3S1554* at 3p21-23, *D5S643* at 5q22-32, *D5S478* at 5p14-15.2 and *D21S1904* at 21p13). We obtained primer sequences for most of the microsatellite markers from the Whitehead Institute for Genome Research and designed those for U20569 based on published sequences of component AP000346 in the GenBank database. There was concordance between deletions detected by QuMA and by array CGH at both the overlapping and adjacent sites (see Web Table A online).

Statistical analysis of the patterns of methylation-and-deletion and gain-and-methylation events. To formally test whether methylation-and-deletion events and gain-and-methylation events were randomly or preferentially distributed among the CpG islands, we first estimated the frequency of methylation and deletion for each tumor. Assuming no preference among sites, the estimated probability of methylation and deletion for any CpG island in a particular tumor is the number of methylation-and-deletion events divided by the number of islands evaluated. The estimated expected frequency of methylation and deletion at a given island for the total of the 26 tumors is the sum of these estimates. Assuming that there is a Poisson distribution of methylation-and-deletion events, and that the occurrence at one site is independent of the occurrence at another site, we calculated the expected number of islands having methylation and deletion on a certain number of tumors and compared that to the observed number (Fig. 3*a*) to create a χ^2 goodness-of-fit statistic. We calculated the *P* value using a Monte Carlo estimate of the exact permutation test *P* value (StatXact).

Drug treatment, reverse transcription, PCR and northern blotting. We plated four glioma cell lines at low density, incubated them with 1 μM 5-aza-2-deoxycytidine for 3 d with fresh drug and medium every 24 h and then isolated total cellular RNA using Trizol (Gibco-BRL). We carried out reverse transcription on RNAs using oligo-dT and random primers. We processed total RNA isolated from brain tissue and primary tumors in a similar fashion.

We did PCR in 25 μl reactions with one-fortieth of each reverse transcription reaction product as template. We amplified the *ACTB* mRNA (encoding β-actin) by incubating the reaction product at 95 °C for 4 min followed by 27 cycles (exponential phase of *ACTB* PCR amplification, data not shown) of 95 °C for 30 s, 68 °C for 30 s and 72 °C for 2 min. We amplified the *COE3* mRNA by incubating the reaction product at 95 °C for 5 min followed by 35 cycles of 95 °C for 1 min, 65 °C for 1 min and 72 °C for 1 min. All primers are available upon request. We used water and genomic DNA as negative controls and detected no PCR products (data not shown). We carried out independent replications of drug treatment, reverse transcription and PCR reactions with similar results.

We also hybridized multiple-human-tissue northern blots (Clontech) sequentially with a *COE3* probe and an *ACTB* probe (see Web Fig. C online). The results confirmed that *COE3* was expressed in normal human brain and most other tissues tested. Because the clinical tumor samples contained variable amounts of blood, we expected that RNA from the tumor samples would be partly derived from blood cells expressing *COE3*.

Bisulfite sequencing method. Briefly, we digested 2.5 μg of DNA from normal tissue and tumor cell line samples with 5 U *Eco*RV and then denatured it in 0.3 M NaOH for 20 min at 42 °C. We added freshly prepared sodium bisulfite (pH 5.0, 208 μl, 3.6 M) and hydroquinone (12 μl, 10 mM) to the denatured DNA in a final volume of 240 μl and then incubated it for 18 h at 55 °C. We then purified DNA using the Promega Wizard DNA Clean-Up System and eluted it in 100 μl of sterilized water. We added freshly prepared NaOH to a final concentration of 0.3 M and incubated samples for 15 min at 37 °C or 20 min at 42 °C. After neutralizing the samples with 3 M ammonium acetate (pH 7), we precipitated and resuspended DNA in 10 μl of sterilized water and stored it at –20 °C until use. We carried out nested PCR on 1 μl of each DNA sample. PCR products were gel purified and cloned into the TOPO TA Cloning/pCR2.1 TOPO kit (Invitrogen). We subjected individual bacterial colonies to PCR using vector-specific primers (sequences available upon request), and the products were sequenced.

URLs. Our custom PERL program used to generate RLGS digestion fragments from the human genome sequence is available at http://shark.ucsf.edu/~stas/Costello/rlgs.html. The August 2001 freeze of the University of California, Santa Cruz version of the draft assembly of human genome is available at http://genome.ucsc.edu. The website for the sequence-tagged site–based map of the Whitehead Institute for Genome Research is http://www-genome.wi.mit.edu/cgi-bin/contig/phys_map.

Note: Supplementary information is available on the Nature Genetics website.

Acknowledgments

We thank the University of California, San Francisco Neurosurgery Tumor Bank for tissue samples, J. Melki for advice on bisulfite sequencing and R. Pieper for critical review of the manuscript. This work was supported by grants from the James S. McDonnell Foundation and the US National Institutes of Health.

Competing interests statement

The authors declare that they have no competing financial interests.

Received 14 June; accepted 20 August 2002.

1. Hatada, I., Hayashizaki, Y., Hirotsune, S., Komatsubara, H. & Mukai, T. A genomic scanning method for higher organisms using restriction sites as landmarks. *Proc. Natl Acad. Sci. USA* **88**, 9523–9527 (1991).
2. Yoshikawa, H. *et al.* Chromosomal assignment of human genomic *Not*I restriction fragments in a two-dimensional electrophoresis profile. *Genomics* **31**, 28–35 (1996).
3. Snijders, A.M. *et al.* Assembly of microarrays for genome-wide measurement of DNA copy number. *Nat. Genet.* **29**, 263–264 (2001).
4. Yoshikawa, H. *et al.* SOCS-1, a negative regulator of the JAK/STAT pathway, is silenced by methylation in human hepatocellular carcinoma and shows growth-suppression activity. *Nat. Genet.* **28**, 29–35 (2001).
5. Makos, M. *et al.* Distinct hypermethylation patterns occur at altered chromosome loci in human lung and colon cancer. *Proc. Natl Acad. Sci. USA* **89**, 1929–1933 (1992).
6. Herman, J.G. *et al.* Silencing of the VHL tumor-suppressor gene by DNA methylation in renal carcinoma. *Proc. Natl Acad. Sci. USA* **91**, 9700–9704 (1994).
7. Jain, A.J. *et al.* Fully automatic quantification of microarray image data. *Genome Res.* **12**, 325–332 (2002).
8. Ginzinger, D.G. *et al.* Measurement of DNA copy number at microsatellite loci using quantitative PCR analysis. *Cancer Res.* **60**, 5405–5409 (2000).
9. Costello, J.F. *et al.* Aberrant CpG-island methylation has non-random and tumor-type-specific patterns. *Nat. Genet.* **24**, 132–138 (2000).
10. Rush, L.J. *et al.* Novel methylation targets in *de novo* acute myeloid leukemia with prevalence of chromosome 11 loci. *Blood* **97**, 3226–3233 (2001).
11. Smiraglia, D.J. *et al.* Excessive CpG island hypermethylation in cancer cell lines versus primary human malignancies. *Hum. Mol. Genet.* **10**, 1413–1419 (2001).
12. Fruhwald, M.C. *et al.* Aberrant promoter methylation of previously unidentified target genes is a common abnormality in medulloblastomas—implications for tumor biology and potential clinical utility. *Oncogene* **20**, 5033–5042 (2001).
13. Dai, Z.Y. *et al.* Global methylation profiling of lung cancer identifies novel methylated genes. *Neoplasia* **3**, 314–323 (2001).
14. Rouillard, J.M. *et al.* Virtual genome scan: a tool for restriction landmark-based scanning of the human genome. *Genome Res.* **11**, 1453–1459 (2001).
15. Starr, R. *et al.* A family of cytokine-inducible inhibitors of signalling. *Nature* **387**, 917–921 (1997).
16. Endo, T.A. *et al.* A new protein containing an SH2 domain that inhibits JAK kinases. *Nature* **387**, 921–924 (1997).
17. Mohapatra, G. *et al.* Genetic analysis of glioblastoma multiforme provides evidence for subgroups within the grade. *Genes Chromosomes Cancer* **21**, 195–206 (1998).
18. Fults, D. & Pedone, C. Deletion mapping of the long arm of chromosome 10 in glioblastoma multiforme. *Genes Chromosomes Cancer* **7**, 173–177 (1993).
19. Karlbom, A.E. *et al.* Loss of heterozygosity in malignant gliomas involves at least three distinct regions on chromosome 10. *Hum. Genet.* **92**, 169–174 (1993).
20. von Deimling, A. *et al.* Comprehensive allelotype and genetic analysis of 466 human nervous system tumors. *J. Neuropathol. Exp. Neurol.* **59**, 544–558 (2000).
21. Dubois, L. & Vincent, A. The COE—Collier/Olf1/EBF—transcription factors: structural conservation and diversity of developmental functions. *Mech. Dev.* **108**, 3–12 (2001).